1   **U-Pb dating of middle Eocene-Pliocene multiple tectonic pulses in the Alpine**

2   **foreland**

4   **Luca Smeraglia[1,2,3], Nathan Looser[4*], Olivier Fabbri[2], Flavien Choulet[2], Marcel Guillong[4],**

5   **Stefano M. Bernasconi[4]**

7   1. National Research Council, IGAG, Rome, Italy

8   2. Chrono-Environnement, UMR 6249, Université de Bourgogne-Franche Comté, 25000 Besançon, France

9   3. formerly at Dipartimento di Scienze della Terra, Sapienza Università di Roma, P.le Aldo Moro 5, 00185, Roma

10   4. Geological Institute, ETH Zürich, Sonneggstrasse 5, 8092 Zürich, Switzerland

12   *Corresponding author e-mail address: Nathan.looser@erdw.ethz.ch

14   **Abstract.** Foreland fold-and-thrust belts record long-lived tectono-sedimentary activity, from passive

15   margin sedimentation, flexuring, and further involvement into wedge accretion ahead of an advancing

16   orogen. Therefore, dating fault activity is fundamental for plate movement reconstruction, resource

17   exploration or earthquake hazard assessment. Here, we report U-Pb ages of syntectonic calcite

18   mineralizations from four thrusts and three tear faults sampled at the regional scale, across the Jura

19   fold-and-thrust belt in the northwestern Alpine foreland (eastern France). Three regional tectonic

20   phases are recognized in the middle Eocene-Pliocene interval: (1) pre-orogenic faulting at 48.4 ± 1.5

21   and 44.7 ± 2.6 Ma associated to the far-field effect of the Alpine compression, (2) syn-orogenic

22   thrusting at 11.4 ± 1.1, 10.6 ± 0.5, 9.7 ± 1.4, 9.6 ± 0.3, and 7.5 ± 1.1 Ma associated to the formation

23   of the Jura fold-and-thrust belt with possible in-sequence thrust propagation, and (3) syn-orogenic

24   tear faulting at 10.5 ± 0.4, 9.1 ± 6.5, 5.7 ± 4.7, and at 4.8 ± 1.7 Ma including the reactivation of a pre-

25   orogenic fault at 3.9 ± 2.9 Ma. Previously unknown faulting events at 48.4 ± 1.5 and 44.7 ± 2.6 Ma

26   predate by ~10 Ma the reported late Eocene age for tectonic activity onset in the Alpine foreland. In

addition, we dated the previously inferred re-activation of pre-orogenic strike-slip faults as tear faults during Jura imbrication. The U-Pb ages document a minimal time frame for the evolution of the Jura FTB wedge by possible in-sequence thrust imbrication above the low-friction basal décollement consisting of evaporites.

1. Introduction

Foreland fold-and-thrust belts develop at the external edges of orogens and are characterized by a multiphase tectono-sedimentary history including: pre-orogenic sedimentation, uplift at the peripheral bulge of the advancing orogen, progressively accelerating subsidence followed by syn-tectonic sedimentation, and accretion of the sedimentary cover into the foreland fold-and-thrust belt (Lacombe et al., 2007). Unraveling the timing of these tectonic events is fundamental for plate kinematic modelling, natural resource exploration, paleoseismicity, and topography evolution studies (Vergés et al., 1992; Craig and Warvakai, 2009). However, deciphering the different tectonic phases is complicated by the overprinting of inherited structures by progressively younger tectonic events.

This issue is addressed by dating syn-tectonic sediments and, more recently, better constrained through dating of fault activity with K-Ar, $^{40}Ar/^{39}Ar$, and U-Pb and U-Th methods (Van der Pluijm et al., 2009; Vrolijk et al., 2018). In particular, calcite U-Pb and U-Th geochronology (Roberts et al., 2020) is the unique method for dating syntectonic calcite mineralizations. This technique has been applied for dating single faults in extensional, strike-slip, and compressional settings (Goodfellow et al., 2017; Nuriel et al., 2017; Hansman et al., 2018; Smeraglia et al., 2019; Carminati et al., 2020). So far, the dating of multiple faults at the regional scale across a foreland fold-and-thrust belt remains rare (Beaudoin et al., 2018; Looser et al., 2021).

In this study, we dated syntectonic calcite mineralizations from four thrusts and three tear faults sampled across the Jura fold-and-thrust belt (Jura FTB, eastern France, Fig. 1) by laser ablation inductively coupled plasma mass spectrometry (LA-ICP-MS) U-Pb dating. We reconstructed three tectonic phases having occurred in the middle Eocene-Pliocene period, documenting a long-lived

polyphase tectonic history of the northwestern Alpine foreland system along the convergent boundary

between European and African plates.
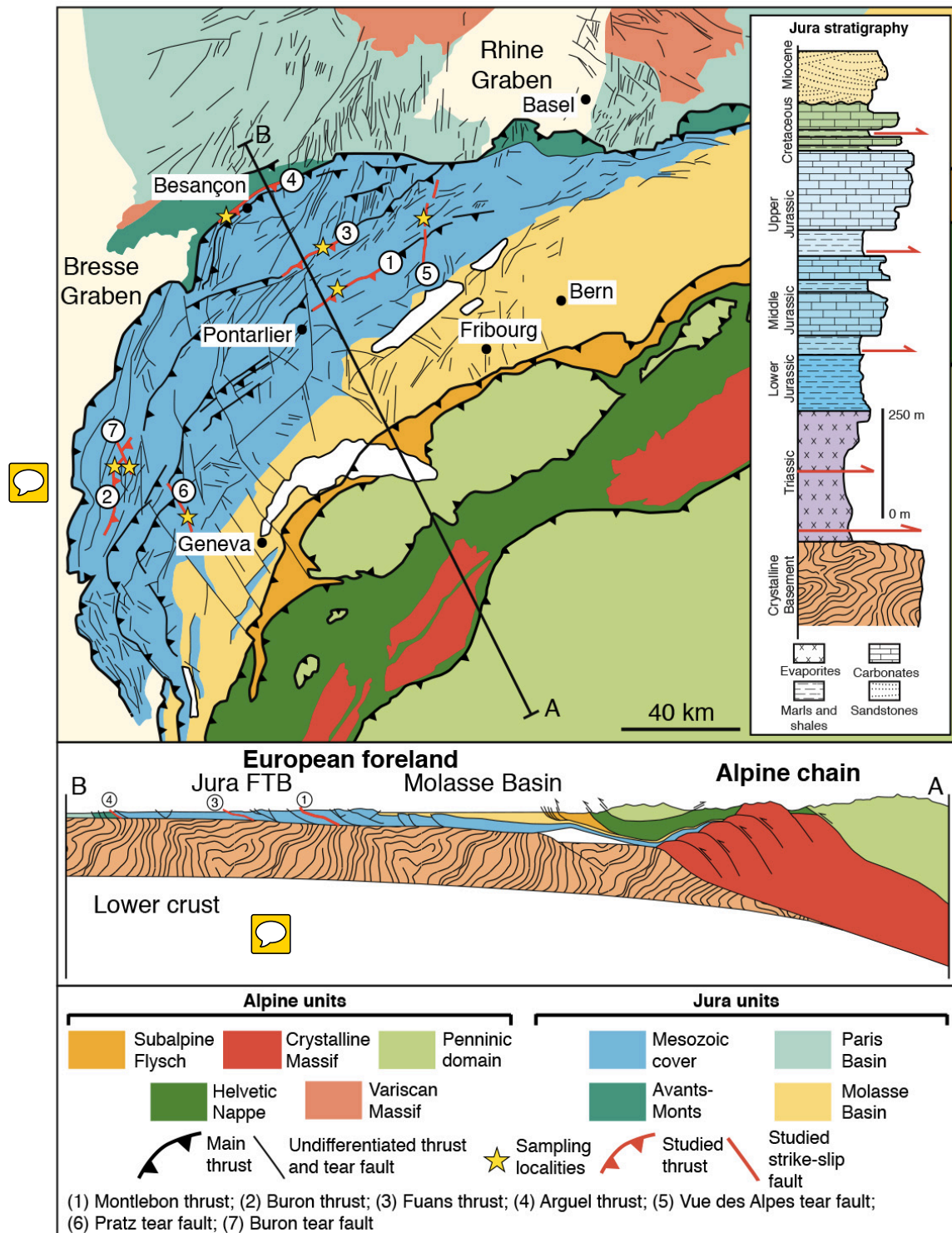
Figure 1. Geological map of the northwestern Alpine foreland and surrounding areas and stratigraphic column of the main lithological units of the Jura area. Modified from Rime et al. (2019).

2. Tectonic setting

The Jura FTB is located in the foreland of the Western Alps and formed by the ongoing continental collision of the Eurasian plate with the African plate (Sommaruga, 1997; Mosar, 1999; Lacombe and Mouthereau, 2002; Affolter and Gratier 2004; Bellahsen et al., 2014) (Fig. 1). Shortening affected the Triassic-late Miocene sedimentary succession deposited on the European passive margin above the Hercynian crystalline basement and caused brittle-ductile deformation at several levels (Fig. 1) (Philippe et al., 1996; Homberg et al., 2002; Ustaszewski and Schmid, 2006). The sedimentary succession starts with Triassic shales and evaporites overlain by Jurassic-Cretaceous shales, marls, and limestones (Fig. 1) (Sommaruga et al., 2017). Following a Late Cretaceous-Eocene regional unconformity, Oligocene-Miocene shallow marine to continental clastic deposits of the Molasse Basin were deposited above Cretaceous limestones (Fig. 1).

The post-Mesozoic tectonic history of the Jura area is assumed to have started in the middle Eocene with N-S shortening related to the far field effect of the "Pyrenean orogeny" generating strike-slip faults (Bergerat, 1987). However, no absolute ages of this tectonic phase are available. Based on structural analyses and calcite U-Pb ages, two phases of normal faulting during the Late Eocene and Oligocene in the distal parts of the Molasse Basin in northern Switzerland have been documented. Normal faulting during the Late Eocene has been related to crustal extension due to the opening of the Rhine Graben, while normal faulting during the middle Miocene has been related to crustal tilting associated to uplift of the Black Forest Highlands and subsidence of the northern part of the Molasse Basin (Mazurek et al., 2018).

Biostratigraphic dating of syn-orogenic deposits, geomorphological observations, interpretation of seismic reflection profiles, and syntectonic calcite U-Pb ages of fault activity in the eastern tip of Jura FTB indicate that orogenic shortening started ~14.5 Ma ago (Langhian times) at the latest (Looser et al., 2021 and references therein) and is still active (Mosar, 1999; Becker, 2000; Madritsch et al., 2008). Shortening was accomodated by N to NE-verging and NE-SW-striking thrusts and by NW-SE to N-S trending sinistral tear faults (Sommaruga, 1997) (Fig. 1). The main

85 décollement level of the thrust system developed along Triassic evaporites (Jordan, 1992; Pfiffner,

86 2014; Gruber, 2017; Sommaruga et al., 2017). Therefore, there is a common agreement in considering

87 the Jura FTB mainly as the product of thin-skinned tectonics (Sommaruga, 1997). However, thick-

88 skinned tectonics occurred in the late stage of deformation and only in the external part (Ustaszewski

89 and Schmid, 2006, 2007; Madritsch et al., 2008; Lacombe and Bellahsen, 2016).

90 Field cross-cutting relationships and U-Pb ages of syntectonic calcite mineralizations show that

91 tear faults were synchronously active with thrusting and folding (Sommaruga, 1997; Looser et al.,

92 2021) and their movement continued after thrusting. In fact, in some cases, tear faults are still

93 seismogenic (Thouvenot et al., 1998). Several authors suggested that pre-orogenic strike-slip and

94 normal faults were reactivated in early Pliocene, respectively as tear and transpressional faults

95 (Madritsch et al., 2008; Homberg et al., 1997; Ustaszewski and Schmid, 2006). Overall, no direct

96 dating of this fault re-activation has been available up to date.

97

98 **3. Methods**

99 The following methods were used: (1) field structural analyses and vein/slickenfiber sampling

100 from four major thrusts (From SE to NW: Montlebon, Buron, Fuans, and Arguel thrusts) and three

101 NNE-SSW tear faults (Vue des Alpes, Pratz, and Buron) moving from the internal (most deformed)

102 to the external (less deformed) parts of the Jura FTB (Fig. 1). In particular, we measured the

103 orientation of sampled veins and the rake of sampled slickenfibers in order to combine U-Pb ages

104 from veins and slickenfibers with structural measurements; (2) microstructural analyses with optical

105 microscope and cathodoluminescence to unravel different phases of calcite precipitation; (3) calcite

106 U-Pb LA-ICP-MS dating on veins and slickenfibers to date fault activity. In most cases, the U-Pb

107 analyses were performed on calcite crystals showing a homogenous color or undisturbed growth-

108 zoning under cathodoluminescence light, indicating no open-system alteration after calcite

109 precipitation by late fluid infiltration and/or recrystallization (Figs. S1-S3). As commonly done in

110 LA-ICP-MS U–Pb carbonate dating, no disequilibrium correction for initial $^{234}U/^{238}U$ and ^{230}Th was

applied. This may cause underestimation of young (<10 Ma) samples (Roberts et al., 2020). Analytical details are described in the Supplementary Material.

4. Results

4.1 Structural and microstructural observations

The Montlebon, Buron, Fuans, and Arguel thrusts are NNE- to SW-NE striking and N- to NW-verging thrusts (Madritsch et al., 2008; Rime et al., 2019; Smeraglia et al., 2020) (Fig. 2a-d). In particular, the Montlebon thrust is characterized by E to ESE-dipping (30-90°) thrust planes with slickenfibers showing left-lateral transpressional movements with N to NNW tectonic transport directions (Fig. 2a). The Buron thrust is characterized by E to SE-dipping (20°-30°) thrust planes with slickenfibers showing left-lateral transpressional movements with NW tectonic transport directions (Fig. 2b). The Fuans thrust is characterized by E to SE-dipping (20°-40°) thrust planes with slickenfibers showing left-lateral transpressional movements with NNW to NW tectonic transport directions (Fig. 2c). The Arguel thrust is characterized by S-dipping (10-30°) thrust planes with slickenfibers showing right-lateral transpressional movements with NNW tectonic transport directions (Fig. 2d).

The subvertical Vue des Alpes, Pratz, and Buron tear faults show a sinistral strike-slip displacement (Sommaruga, 1997) (Fig. 2de-g). In particular, the Vue des Alpes strike-slip fault is characterized by NE-SW-striking subvertical fault planes with slickenfibers showing sinistral movements and associated NW-SE-striking subvertical fault planes with slickenfibers showing dextral movements (Fig. 2e). Both the Pratz and Buron strike-slip faults are characterized by NE-SW-striking subvertical fault planes with slickenfibers showing sinistral movements (Fig. 2f-g).
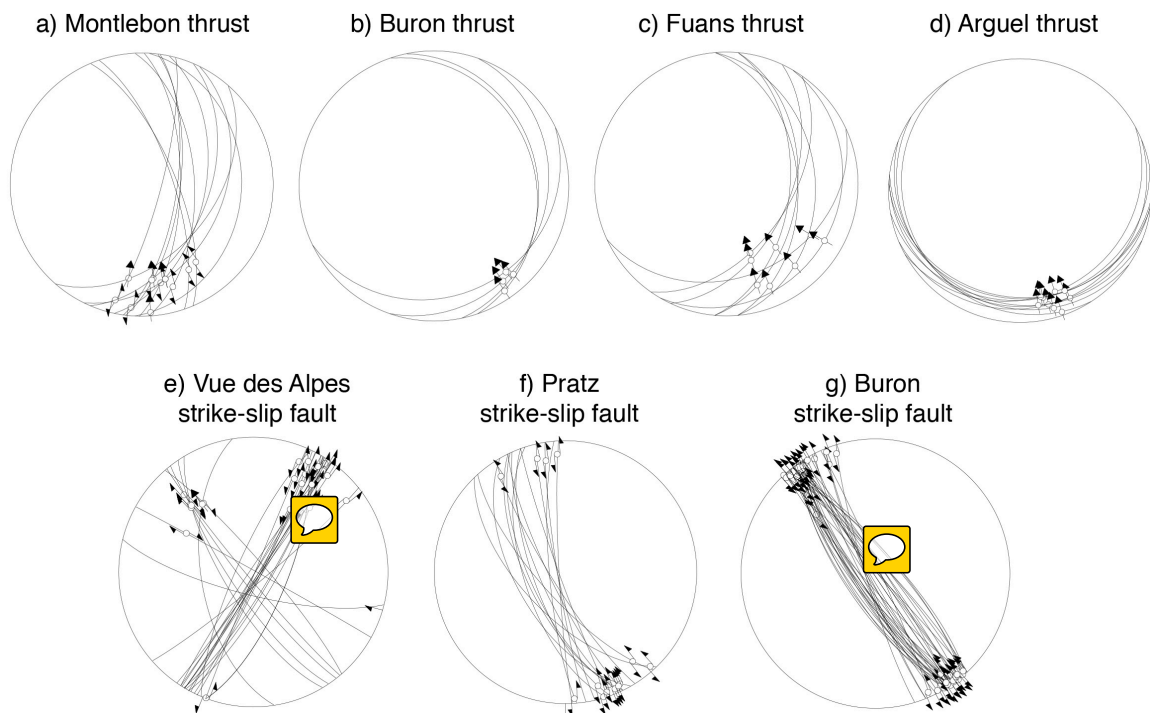
Figure 2. Lower Schmidt hemisphere projection of fault-slip data and slip vectors for thrust and strike-slip faults. **(a)** Montlebon thrust. **(b)** Buron thrust. **(c)** Fuans thrust. **(d)** Arguel thrust. **(e)** Vue des Alpes strike-slip fault. **(f)** Pratz strike-slip fault. **(g)** Buron strike-slip fault-

Both thrusts and strike-slip faults cut through Middle-Upper Jurassic and Lower Cretaceous limestones. The fault core zones are characterized by foliated fault rocks cut by sharp fault planes (Fig. 3a-d). Breccia lenses are developed in the Buron thrust core (Fig. 4d). Calcite mineralizations in extensional veins (Buron, Arguel, Montlebon, Vue des Alpes, and Pratz) and in slickenfibers (Fuans, Vue des Alpes, and Pratz) were sampled.

Extensional veins occur in limestone fragments of foliated fault rocks (Fig. 3e,g) and in clasts from breccias (Figs. 3f and 4g). In limestone fragments of foliated fault rocks, extensional veins are oriented perpendicularly to stylolites (Fig. 3e,g), which occur along S- and C-planes. Extensional veins in clasts from breccias show a crackle-like texture and mutually cross-cutting relationships (Fig. 3f). Extensional veins are filled by blocky to elongated-blocky calcite crystals and show syntaxial growth (Figs. 3i-k, 4g, S1a-d, S2a,b,g,h, S3a-h).

149   The fault planes are coated by slickenfibers (Figs. 3d,h and 4e,f). At the microscale,

150   slickenfibers occur in dilational jogs along shear planes (Fig. 3h) and are filled by fibrous calcite

151   crystals bounded by sharp shear planes (Figs. 3j, 4i, S1e-h, and S2c-f) and/or by blocky calcite crystals

152   (Figs. 3l and 4h). Fibrous crystals are oriented parallel to shear planes.

153   Most of the studied veins and slickenfibers show homogeneous cathodoluminescence colors,

154   ranging from bright to dull red, and/or show cathodoluminescence zoning on the same crystal (Figs.

155   3i-l, 4g-i, S1a,c,e,g, S2a,c,e,g, and S3a,c,e,g). In places, slickenfibers and extensional veins are cross-

156   cut by extensional veins showing black to dull red luminescence colors (Figs. S1e-h, S2c-f, and

157   S3a,b,g,h)
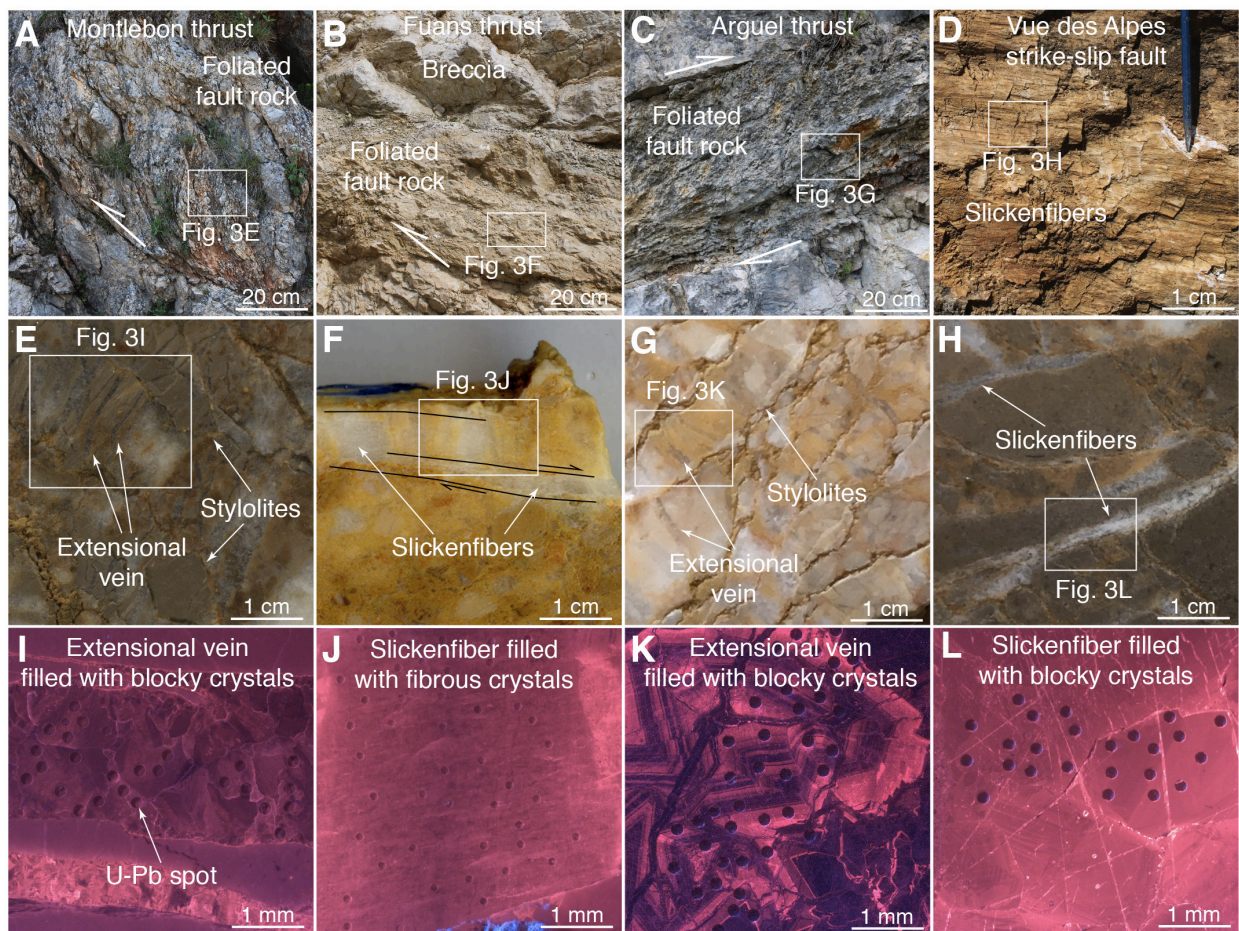
158

159   **Figure 3.** Foliated fault rocks in the fault core of the Montlebon thrust **(a)**, Arguel thrust **(b)**, and **(c)** Fuans thrust. **(d)**

160   Detail of minor fault plane along the Vue des Alpes strike-slip fault showing calcite slickenfibers. **(e)** Hand sample from

161   the Montlebon thrust showing host rock sigmoids bounded by stylolites and extensional veins perpendicular to stylolites.

162   **(f)** Hand sample from the Fuans thrust showing host rock sigmoids bounded by stylolites and extensional veins

perpendicular to stylolites. **(g)** Hand sample from the Arguel thrust showing extensional veins with crackle-like texture. **(h)** Hand sample from a minor fault plane along the Vue des Alpes strike-slip fault showing slickenfibers developed along dissolution planes. **(i-l)** Cathodoluminescence microphotographs of thin sections showing extensional veins and slickenfibers from the studied faults with ablation craters of the U-Pb analyses.
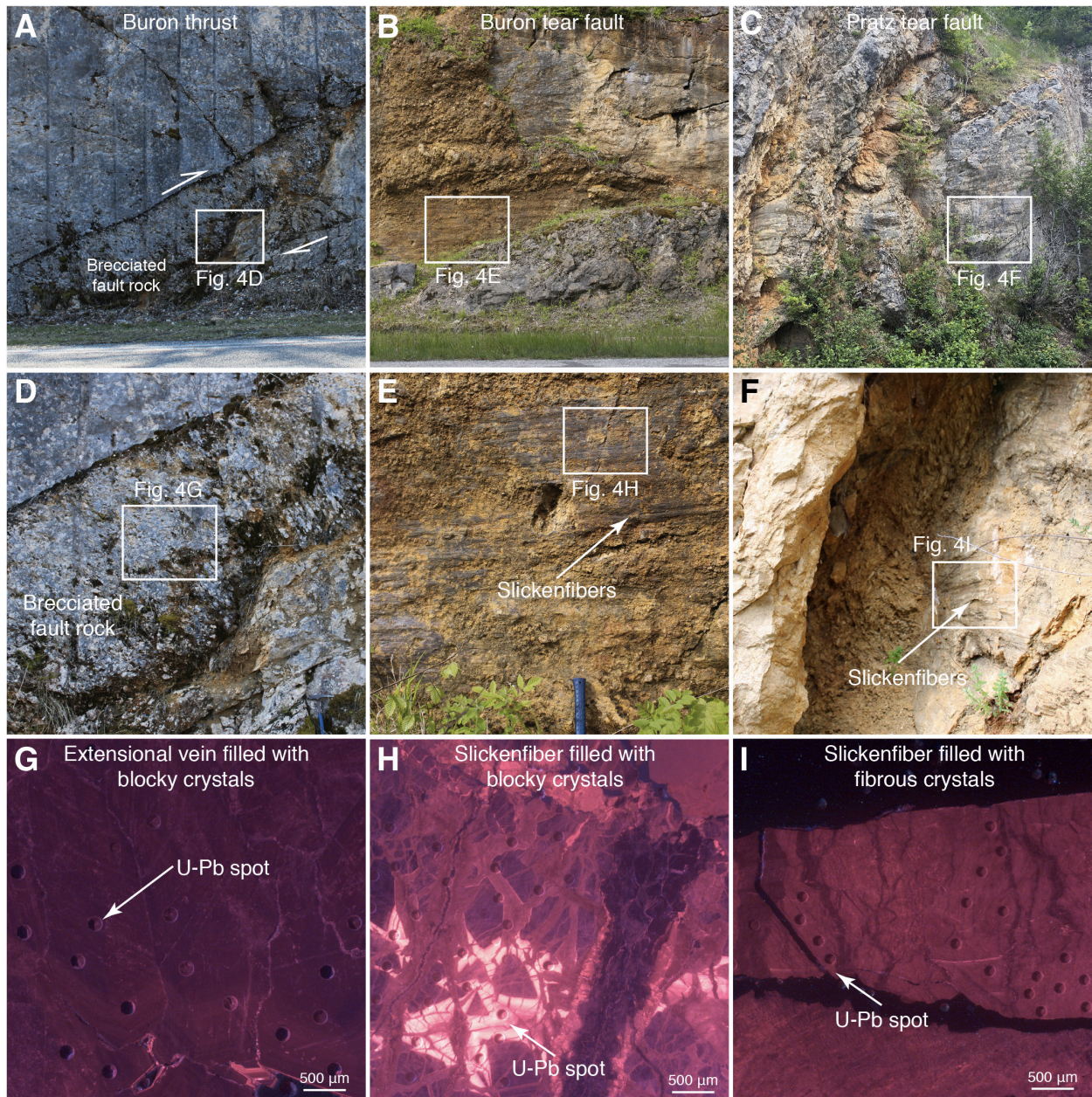
Figure 4. (a) Buron thrust. **(b)** Buron tear fault. **(c)** Pratz tear fault. **(d)** Brecciated fault rocks in the fault core of the Buron thrust. **(e)** Brecciated fault rocks cut by sharp fault planes in the fault core of the Buron tear fault. **(f)** Foliated fault rock cut by sharp fault planes in the fault core of the Pratz tear fault. **(g-i)** Cathodoluminescence microphotographs of

172 thin sections showing extensional veins and slickenfibers from the studied faults with ablation craters of the U-Pb

173 analyses.

174

175 *4. 2 U-Pb dating*

176 A total of 12 reliable lower intercept ages (Figs. 5 and 6) out of 19 analyses (rejected age data

177 is presented in Fig. S4) are reported with uncertainties at 2σ absolute including counting statistics

178 uncertainties, uncertainty of the primary reference material and inter-session variations (Guillong et

179 al., 2020). The U-Pb ages indicate different phases of tectonic activity and related calcite precipitation

180 in the middle Eocene to Pliocene period and also multiple precipitation ages along the same fault

181 (Supplementary Information Table 1).

182 An extensional vein from the Montlebon thrust shows a Serravallian age of 11.4 ± 1.1 Ma (Fig.

183 5a). An extensional vein from the Buron thrust shows a Tortonian age of 10.6 ± 0.5 Ma (Fig. 5b).

184 Two slickenfibers from the Fuans thrust yield Tortonian ages indistinguishable from each other of

185 9.7 ± 1.4 Ma and 9.6 ± 0.3, respectively (Fig. 5c,d). An extensional vein from the Arguel thrust shows

186 a Tortonian-Messinian age of 7.5 ± 1.1 Ma (Fig. 5e). Along the Vue des Alpes strike-slip fault, two

187 slickenfibers yield Ypresian-Lutetian ages of 44.7 ± 2.6 and 48.4 ± 1.5 Ma (Fig. 6a,b), while an

188 extensional vein shows a Pliocene age of 3.9 ± 2.9 Ma (Fig. 6c). An extensional vein from the Buron

189 strike-slip fault shows a Messinian age of 5.7 ± 4.7 Ma (Fig. 6d). One slickenfiber and one extensional

190 vein from the Pratz strike-slip fault show Tortonian-Messinian ages of 10.5 ± 0.4 and 9.1 ± 6.5 Ma

191 (Fig. 6f-g), while one slickenfiber shows a younger age of 4.8 ± 1.7 Ma (Fig. 6e). Because of the

192 common-lead rich $^{207}Pb/^{206}Pb$ compositions, the U-Pb ages of the samples DA2, BUS1, PR1-A, PR2-

193 2 of the strike-slip faults have larger uncertainties than those of the thrusts.

194

195

U-Pb ages from thrusts
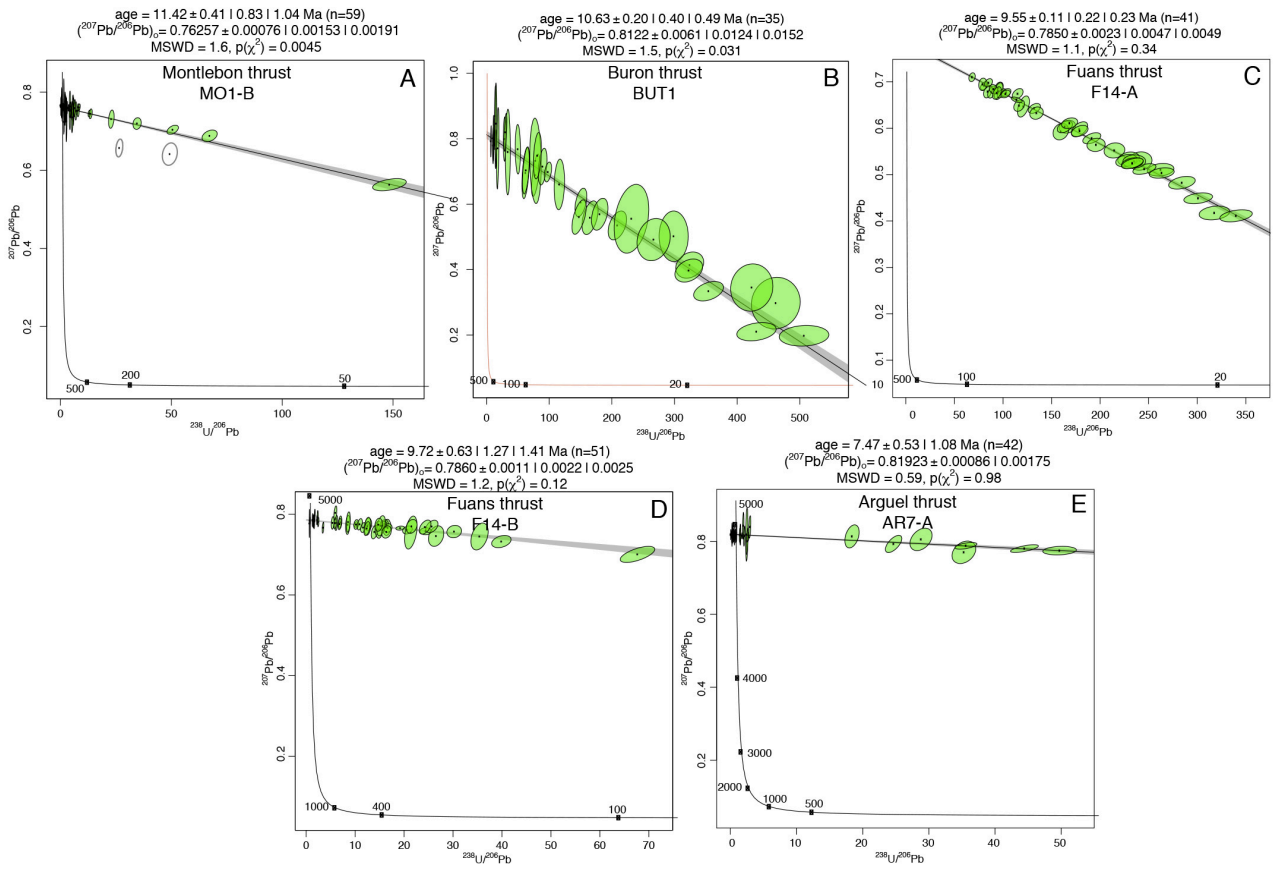
Figure 5. Tera-Wasserburg concordia diagrams of thrust faults. **(a)** Montlebon thrust. **(a)** Buron thrust. **(c,d)** Fuans thrust. **(e)** Arguel thrust.

199

U-Pb ages from strike-slip faults

200
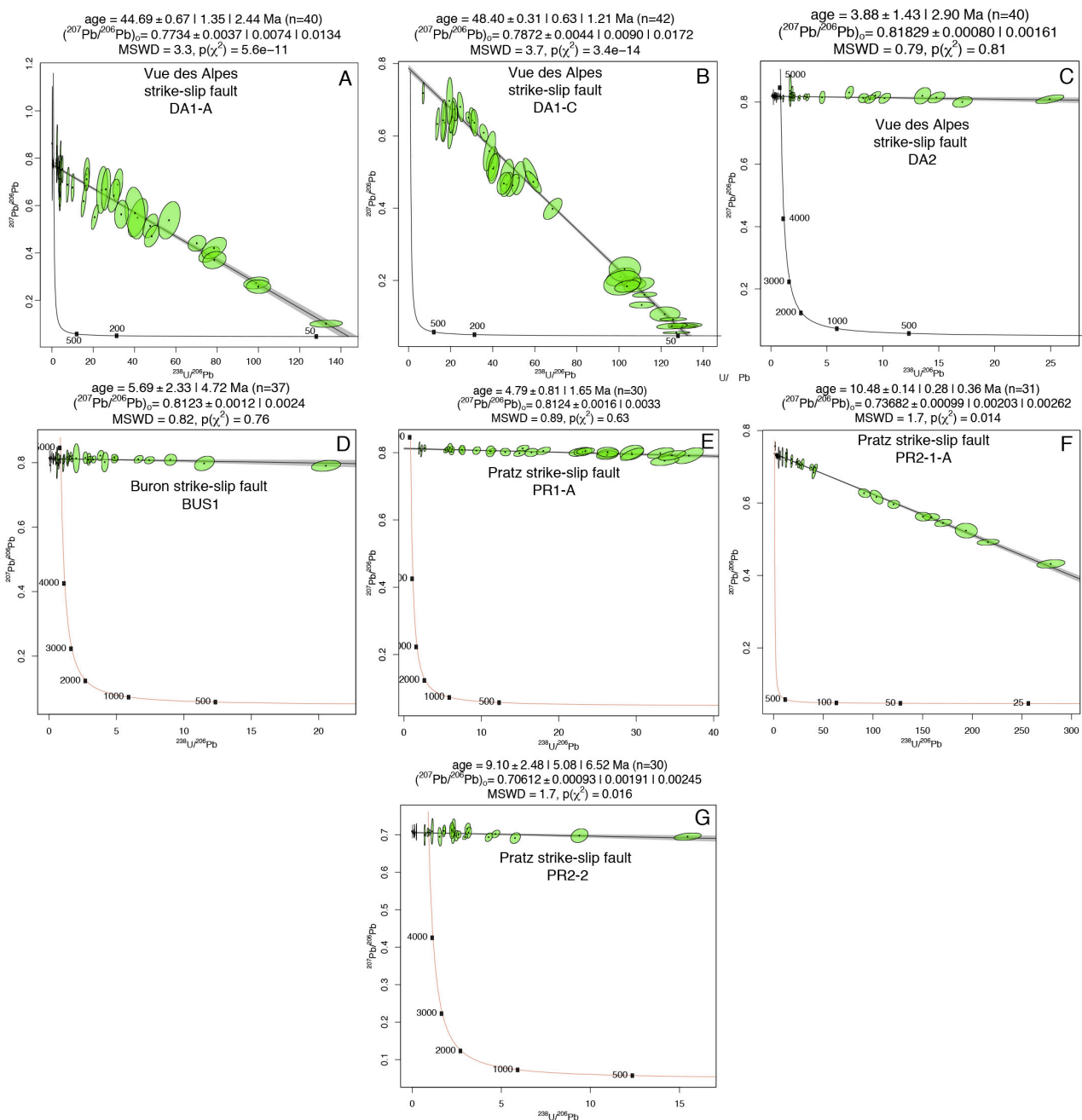
Figure 6. Tera-Wasserburg concordia diagrams of strike-slip faults. **(a-c)** Vue des Alpes strike-slip fault. **(d)** Buron strike-

slip fault. **(e-g)** Pratz strike-slip fault.

203

5. Discussion and conclusions

205   Slickenfibers on sharp fault planes are clear evidence of tectonic slip along faults (Figs. 3j-l, 4i,

206   S1e-h, and S2c,f). In particular, blocky and fibrous crystals indicate respectively fast and slow vein

207   opening rates associated with fault slip. Within slickenfibers, calcite crystal precipitated during syn-

208   to early post-slip fluid influx in newly formed dilational sites formed along undulated and sharp slip

209   planes (Gratier and Gamond, 1990; Urai et al., 1991; Holland and Urai, 2010; Fagereng et al., 2010;

210   Bons et al., 2012; Woodcock et al., 2014). Extensional veins oriented perpendicular to stylolites (Fig.

211   3e,g) are linked to syn-thrusting shortening (Gratier et al., 2013). The studied veins are therefore

212   interpreted as the product of tectonic fault slip and their U-Pb ages are considered as representative

213   of faulting activity.

214   We recognize three regional tectonic phases between the middle Eocene and the Pliocene (Figs.

215   7 and 8) which are linked to the long-lived tectonic activity of the Alpine foreland evolution. The

216   presented ages should be regarded as minimum ages for the onset of deformation at the studied faults

217   or as maximum ages for its termination as potentially older or younger deformation phases recorded

218   by other veins and slickenfibers not sampled and analyzed here may have been missed.

219   The U-Pb ages are regionally consistent in terms of tectonic evolution of the Jura FTB and the

220   microstructures of the analyzed veins and slickenfibers indicate precipitation during syn- to early

221   post-slip fluid influx. However, although U-Pb dating was performed on crystals with no indication

222   of later open-system alteration based on CL-microscopy, possible late fluid infiltration and calcite

223   recrystallization cannot be excluded as previously suggested by other studies (Beaudoin et al., 2018;

224   Hoareau et al., 2021; Roberts et al., 2020, 2021).

225   Sample BUS1 clearly shows multiple calcite phases indicating vein re-opening and potentially

226   different ages (Fig. 4h). However, the Tera-Wasserburg diagram of BUS1 shows a single age trend

227   with a low MSWD of 0.82 (Fig. 6d). This would not be observed in a sample that experienced

228   crystallization at significantly different times. Therefore, sample BUS1 reflects calcite precipitation

229   within a time interval smaller than what would result in multiple age trends.

230   The oldest tectonic phase is recorded by two horizontal slickenfibers dated at 44.7 ± 2.6 and

231   48.4 ± 1.5 Ma in Ypresian-Lutetian times (middle Eocene) along the Vue des Alpes strike-slip fault

232   (Fig. 7). These ages are ~10 Ma older than the onset of the extensional tectonic activity in Priabonian

233   (late Eocene) related to Rhine Graben opening (Sissingh, 1998; Mazurek et al. 2018). The strike-slip

234   faulting in Eocene times is consistent with fault-slip data of Homberg et al. (1997). We propose that

235   the Ypresian-Lutetian tectonic activity can be related to the late Mesozoic-Eocene far field tectonic

236   shortening in the European plate foreland due to the advancing Alpine orogen (Mazurek et al., 2006;

237   Timar-Geng et al., 2006) (Fig. 8a). On the contrary, previous studies suggested that middle Eocene

238   strike-slip faulting in the Jura area was related to the far-field effect of the Pyrenean compression

239   (Bergerat, 1987; Homberg et al., 2002). The Pyrenean far field effect has also been recognized in the

240   Paris Basin (eg, Lacombe et al., 1990; Lacombe and Mouthereau, 1999; Lacombe and Obert, 2000),

241   in eastern France (Lacombe et al., 1993), and even in the UK (Hibsch et al., 1995) where Pyrenean-

242   related calcite veins were dated by U-Pb (Parrish et al., 2018). However, even though tectonic stresses

243   have been shown to be transmitted more than thousand km away from the orogenic front (Craddock

244   et al., 1993; Beaudoin and Lacombe, 2018), further studies are necessary to better constrain the origin

245   of pre-Miocene fault activity in the European foreland.

246   Structural analyses of the studied thrusts highlight N to NW oriented tectonic transport

247   directions (Fig. 4a-d) consistent with the regional NW-SE to N-S compressional phase that has

248   affected the Jura fold and thrust belt since the Miocene (Philippe et al, 1996; Becker, 2000; Homberg

249   et al., 2002; Ustaszewski and Schmid, 2006; Madritsch et al., 2008; Looser et al., 2021). Although

250   age uncertainties do not allow a distinction beyond doubt and the limited numbers of U-Pb ages and

251   studied thrusts provide a limited picture, the Jura imbrication seems to have occurred by in-sequence

252   thrusting. The oldest observed thrusts ages are Serravallian-Messinian and become progressively

253   younger moving from the inner (SE) toward the external (NW) part, from 11.4 ± 1.1, 10.6 ± 0.5, 9.7

254   ± 1.4 and 9.6 ± 0.3 on the same thrust, and 7.5 ± 1.1 Ma, respectively, in the Montlebon, Buron,

255   Fuans, and Arguel thrusts (Figs. 7 and 8b). These ages are consistent with the time interval of ~14.5-

256   3.3 Ma suggested for thrusting activity from biostratigraphic dating of syn- to post-tectonic sediments

257   (Becker, 2000 and references therein) and from calcite U-Pb ages of thrust activity in the eastern Jura

258   FTB (Looser et al., 2021) (Fig. 7).

259   Previous studies interpreted the subvertical strike-slip faults in the Jura FTB as tear faults, with

260   activity during thrusting and folding (Sommaruga, 1997; Looser et al., 2021). Our structural analyses

261   and U-Pb ages from the studied strike-slip faults support this interpretation. In particular, strike-slip

262   faults are subvertical and are roughly parallel or oblique to the regional transport directions inferred

263   from thrust kinematics (compare tectonic transport directions of Fig. 4a-d with those of Fig. 4f,g), a

264   common feature of tear faults (Twiss and Moores, 1992).

265   The Buron thrust, active at 10.6 ± 0.5 Ma, was cross-cut by the Buron tear fault ~5 Ma later, at

266   5.7 ± 4.7 Ma (Figs. 7 and 8c). The Pratz tear fault was active at 10.5 ± 0.4 and 9.1 ± 6.5 Ma, indicating

267   tear faulting generation during coeval thrust propagation, and further late-orogenic re-activation at

268   4.8 ± 1.7 Ma (Figs. 7 and 8b). These data indicate that tear faulting occurred during syn- to late-

269   orogenic times (Fig. 8b,c). In addition, a late-orogenic phase is recorded by an extensional vein from

270   the Vue des Alpes strike-slip fault showing a Pliocene age of 3.9 ± 2.9 Ma (Fig. 7). This age has been

271   measured on an extensional vein that cannot be directly related to fault slip. Therefore, we cannot

272   completely exclude that this age represents a late alteration event not directly linked to fault slip

273   during the Pliocene. However, the 3.9 ± 2.9 Ma age is consistent with late orogenic deformation

274   between 4.2 and 2.9 Ma documented in the frontal part of the Jura FTB (Madritsch et al., 2008 and

275   references therein). The 3.9 ± 2.9 Ma age from the Vue des Alpes strike-slip fault is ~40 Ma younger

276   than the middle Eocene ages (44.7 ± 2.6 and 48.4 ± 1.5 Ma) measured on the same fault, suggesting

277   the reactivation of the Vue des Alpes strike-slip fault during late Jura shortening. This inference is

278   also consistent with field cross-cutting relationships indicating re-activation of pre-existing strike-

279   slip faults as tear faults (Homberg et al., 1997).

280   We consider the retrieved age as fault re-activation of the Vue des Alpes strike-slip fault and

281   relate it to a stress change from pure compression to strike-slip state of stress coupled with the

occurrence of an inherited strike-slip fault favorably oriented with respect to the regional stress field. This stress change associated with tear fault development can be related to progressive fold-and-thrust belt thickening and erosion initiating only after ~4.5 M (Looser et al., 2021 and references therein), which led to an increase in the maximum vertical stress (sigma 3) and a switch between sigma 3 and 2 (Ferril et al., 2021). Shortening is still active in the Jura FTB and tear faults (also re-activated tear faults) are seismogenic (Thouvenot et al., 1998).

The presented tectonic reconstruction depicts a stable evolution of the Jura FTB wedge by possible in-sequence thrusting consistent with thrust imbrication above the low-friction décollement consisting of evaporites (Fig. 8a-c). Contrarily, out-of-sequence thrusting occurred as late as in Messinian-early Pliocene times in the proximal Molasse Basin (Von Hagke et al., 2012, 2014) and in the Alps (Bellahsen et al., 2014). This tectonic framework suggests a stable topographic evolution of the critical taper and topographic profile of the Jura fold-and-thrust belt. Finally, this study constrains a long-lived polyphase tectonic history of the northwestern Alpine foreland system along the convergent boundary between European and African plates from the middle Eocene to the Pliocene.
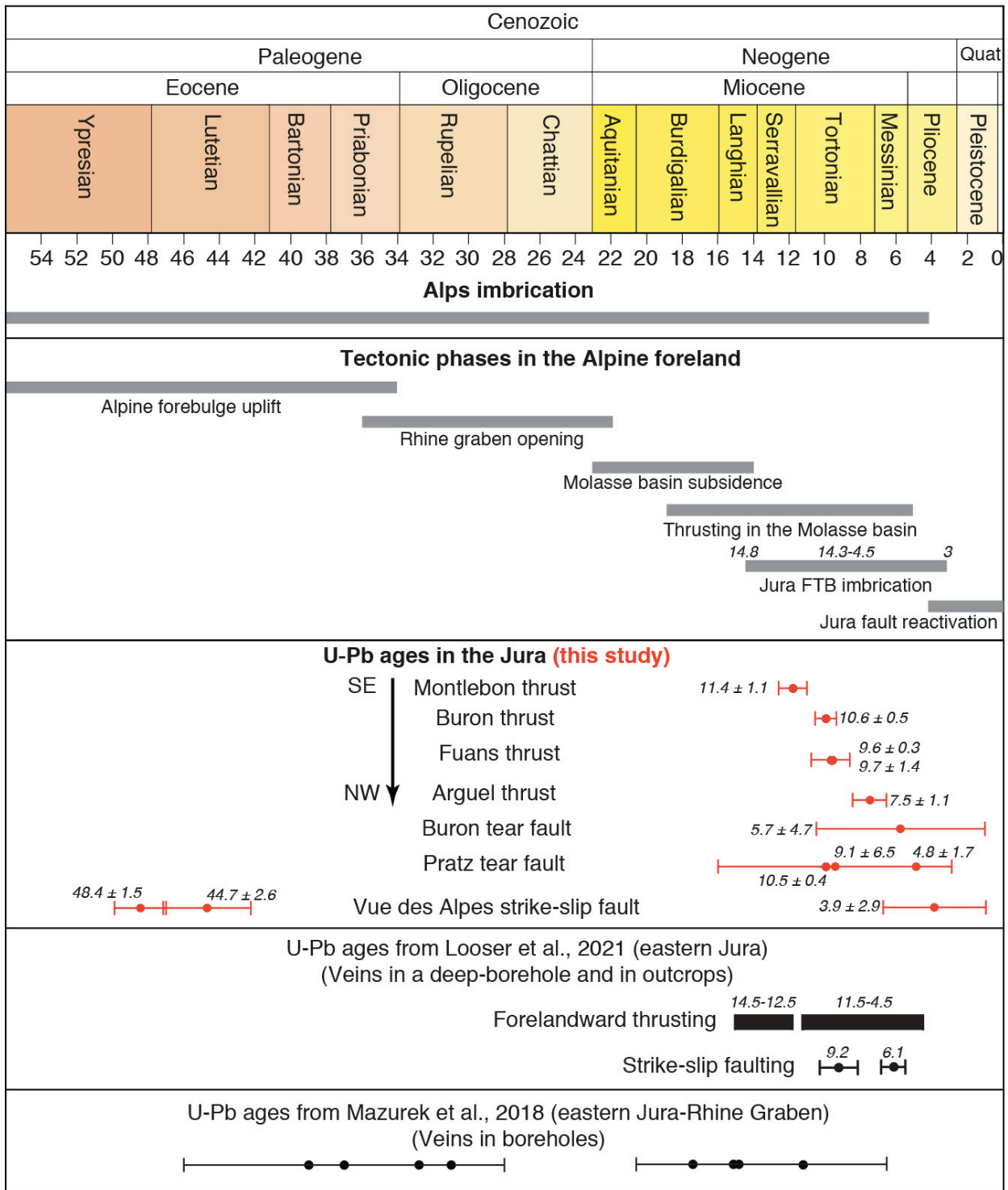
Figure 7. Main tectonic phases in the Alps and in the Alpine foreland. Age constraints shown as grey bars are from Burkhard and Sommaruga (1998), Ustaszewski et al. (2006), Madritsch et al. (2008), Bellahsen et al. (2014), and Von Hagke et al. (2014). For calcite U-Pb data, all uncertainties are represented as 2σ.

A) Ypresian-Lutetian (middle Eocene)
Far field tectonic effect of Alpine orogen

Europe-Africa convergence

1) Strike-slip faulting in the
Vue des Alpes (44.7 ± 2.6; 48.4 ± 1.5 Ma)

B) Serravallian-Messinian (middle-late Miocene)
Jura fold-and-thrust belt accretion

Younger thrust ages

Jura shortening

Europe-Africa convergence

Thrusting in the
Molasse basin

2) Montlebon thrust (11.4 ± 1.1 Ma)
3) Buron thrust (10.6 ± 0.5 Ma)
4) Fuans thrust (9.6 ± 0.3; 9.7 ± 1.4 Ma)
5) Arguel thrust (7.5 ± 1.1 Ma)
6) Pratz tear fault (10.5 ± 0.4; 9.1 ± 6.5)

C) late Miocene-middle Pliocene
Tear fault reactivation in the Jura fold-and-thrust belt

Europe-Africa convergence

7) Buron tear fault (5.7 ± 4.7 Ma)
8) Re-activation of Pratz tear fault (4.8 ± 1.7)
9) Re-activation of Vue des Alpes strike-slip fault (3.9 ± 2.9 Ma)

Mesozoic cover	Molasse Basin	Alpine units	Crystalline basement

300

301 **Figure 8. (a-d)** Schematic reconstruction of the main tectonic phases dated in the Jura area in the regional context of the

302 Alpine foreland system evolution.

303

ACKNOWLEDGEMENT

We thank CASP (https://www.casp.org.uk/) for financial support during fieldwork activity by the Andy Whitham Fieldwork Award 2019 to L. Smeraglia. Financial support by Borsa di Perfezionamento Estero 2017 (Sapienza) to L. Smeraglia, UMR 6249 and OSU Theta projects to O. Fabbri and F. Choulet are acknowledged. U-Pb analyses were funded by the Swiss National Science Foundation project number 200021_169849 to S. M. Bernasconi. We thank J. Mosar, M. Schori, A. Sommaruga, C. Mottran, L. Weiss, and C. Von Hagke for constructive discussions and suggestions, also during fieldwork. We thank the Editor Susanne Buiter and two Reviewers Olivier Lacombe and Nick Roberts for their constructive comments that helped to improve the manuscript.

REFERENCES

Affolter, T., and Gratier, J. P.: Map view retrodeformation of an arcuate fold-and-thrust belt: The Jura case. Journal of Geophysical Research: Solid Earth, 109(B3), 2004.

Beaudoin, N., and Lacombe, O.: Recent and future trends in paleopiezometry in the diagenetic domain: Insights into the tectonic paleostress and burial depth history of fold-and-thrust belts and sedimentary basins. Journal of Structural Geology, 114, 357-365, 2018.

Beaudoin, N., Leprêtre, R., Bellahsen, N., Lacombe, O., Amrouch, K., Callot, J. P., ... and Daniel, J. M.: Structural and microstructural evolution of the Rattlesnake Mountain Anticline (Wyoming, USA): new insights into the Sevier and Laramide orogenic stress build-up in the Bighorn Basin. Tectonophysics, 576, 20-45, 2012.

Beaudoin, N., Lacombe, O., Roberts, N. M., and Koehn, D.: U-Pb dating of calcite veins reveals complex stress evolution and thrust sequence in the Bighorn Basin, Wyoming, USA. Geology, 46(11), 1015-1018, 2018.

Becker, A.: The Jura Mountains - an active foreland fold-and-thrust belt?. Tectonophysics, 321(4), 381-406, 2000.

329   Bellahsen, N., Mouthereau, F., Boutoux, A., Bellanger, M., Lacombe, O., Jolivet, L., and Rolland,

330   Y. : Collision kinematics in the western external Alps. Tectonics, 33(6), 1055-1088, 2014.

331   Bergerat, F.: Stress fields in the European platform at the time of Africa-Eurasia collision. Tectonics

332   6, 99-132, 1987.

333   Bons, P. D., Elburg, M. A., and Gomez-Rivas, E.: A review of the formation of tectonic veins and

334   their microstructures. Journal of Structural Geology, 43, 33-62, 2012.

335   Carminati E., Aldega L., Smeraglia L., Scharf A., Mattern F., Albert R., and Gerdes A.: Tectonic

336   evolution of the Northern Oman Mountains, part of the Straits of Hormuz Syntaxis: new

337   structural and paleothermal analyses and U-Pb dating of synkinematic calcite. Tectonics 39,

338   e2019TC005936, 2020.

339   Craig, M. S., and Warvakai, K.: Structure of an active foreland fold and thrust belt, Papua New

340   Guinea. Australian Journal of Earth Sciences, 56(5), 719-738, 2009.

341   Craddock, J. P., Jackson, M., van der Pluijm, B. A., & Versical, R. T.: Regional shortening fabrics in

342   eastern North America: Far-field stress transmission from the Appalachian-Ouachita Orogenic

343   Belt. Tectonics, 12(1), 257-264, 1993.

344   Fagereng, Å., Remitti, F., and Sibson, R. H.: Shear veins observed within anisotropic fabric at high

345   angles to the maximum compressive stress. Nature Geoscience, 3(7), 482, 2010.

346   Ferril, D.A., Smart, K.J., Cawood, A.J., Morris, A.P.: The fold-thrust belt stress cycle: Superposition

347   of normal, strike-slip, and thrust faulting deformation regimes. Journal of Structural Geology

348   148, 104362, 2021.

349   Goodfellow, B. W., Viola, G., Bingen, B., Nuriel, P., and Kylander-Clark, A. R.: Paleocene faulting

350   in SE Sweden from U–Pb dating of slickenfiber calcite. Terra Nova, 29(5), 321-328, 2017.

351   Gratier, J. P., and Gamond, J. F.: Transition between seismic and aseismic deformation in the upper

352   crust. Geological Society, London, Special Publications, 54(1), 461-473, 1990.

353 Gratier, J.P., Thouvenot, F., Jenatton, L., Tourette, A., Doan, M.L., Renard, F.: Geological control of

354   the partitioning between seismic and aseismic sliding behaviours in active faults: evidence from

355   the Western Alps, France. Tectonophysics 600, 226-242, 2013.

356 Gruber, M.: Structural Investigations of the Western Swiss Molasse Basin - From 2D Seismic

357   Interpretaion to a 3D Geological Model. GeoFocus, 41, 190 pp, 2017.

358 Guillong, M., Wotzlaw, J., Looser, N., & Laurent, O. (2020). Evaluating the reliability of U–Pb laser

359   ablation inductively coupled plasma mass spectrometry (LA-ICP-MS) carbonate

360   geochronology: Matrix issues and a potential calcite validation reference material.

361   Geochronology, 2, 155–167. https://doi.org/10.5194/gchron-2-155-2020.

362 Hansman, R. J., Albert, R., Gerdes, A., and Ring, U.: Absolute ages of multiple generations of brittle

363   structures by U-Pb dating of calcite. Geology, 46(3), 207-210, 2018.

364 Hibsch, C., Jarrige, J. J., Cushing, E. M., and Mercier, J.: Palaeostress analysis, a contribution to the

365   understanding of basin tectonics and geodynamic evolution. Example of the Permian/Cenozoic

366   tectonics of Great Britain and geodynamic implications in western Europe. Tectonophysics,

367   252(1-4), 103-136, 1995.

368 Hoareau, G., Crognier, N., Lacroix, B., Aubourg, C., Roberts, N. M., Niemi, N., ... and Ruiz, I. S.:

369   Combination of Δ47 and U-Pb dating in tectonic calcite veins unravel the last pulses related to

370   the Pyrenean Shortening (Spain). Earth and Planetary Science Letters, 553, 116636, 2021.

371 Holland, M., and Urai, J. L.: Evolution of anastomosing crack–seal vein networks in limestones:

372   Insight from an exhumed high-pressure cell, Jabal Shams, Oman Mountains. Journal of

373   Structural Geology, 32(9), 1279-1290, 2010.

374 Homberg, C., Hu, J. C., Angelier, J., Bergerat, F., and Lacombe, O.: Characterization of stress

375   perturbations near major fault zones: insights from 2-D distinct-element numerical modelling

376   and field studies (Jura mountains). Journal of Structural Geology, 19(5), 703-718, 1997.

377   Homberg, C., Bergerat, F., Philippe, Y., Lacombe, O., and Angelier, J.: Structural inheritance and

378   Cenozoic stress fields in the Jura fold-and-thrust belt (France). Tectonophysics, 357(1-4), 137-

379   158, 2002.

380   Jordan, P.: Evidence for large-scale decoupling in the Triassic evaporites of Northern Switzerland:

381   an overview. Eclogae Geologicae Helvetiae, 85, 677–693, 1992.

382   Lacombe, O., Angelier, J., Laurent, P., Bergerat, F., and Tourneret, C.: Joint analyses of calcite twins

383   and fault slips as a key for deciphering polyphase tectonics: Burgundy as a case study.

384   Tectonophysics, 182(3-4), 279-300, 1990.

385   Lacombe, O., Angelier, J., Byrne, D., and Dupin, J. M.: Eocene-Oligocene tectonics and kinematics

386   of the Rhine-Saone continental transform zone (eastern France). Tectonics, 12(4), 874-888,

387   1993.

388   Lacombe, O., and Mouthereau, F.: What is the real front of orogens? The Pyrenean orogen as a case

389   study. Comptes Rendus de l'Academie des Sciences Series IIA Earth and Planetary Science,

390   329(12), 889-896, 1999.

391   Lacombe, O., & Mouthereau, F. (2002). Basement-involved shortening and deep detachment

392   tectonics in forelands of orogens: Insights from recent collision belts (Taiwan, Western Alps,

393   Pyrenees). *Tectonics*, *21*(4), 12-1.

394   Lacombe, O., and Obert, D.: Structural inheritance and cover deformation: Tertiary folding and

395   faulting in, the western Paris Basin. Comptes rendus de l'academie des sciences serie ii

396   fascicule a-sciences de la terre et des planetes, 330(11), 793-798, 2000.

397   Lacombe, O., Lavé, J., Roure, F. M., and Vergés, J. (Eds.).: Thrust belts and foreland basins: From

398   fold kinematics to hydrocarbon systems. Springer Science & Business Media, 2007.

399   Lacombe, O., and Bellahsen, N.: Thick-skinned tectonics and basement-involved fold–thrust belts:

400   insights from selected Cenozoic orogens. Geological Magazine, 153, 763-810, 2016.

401   Looser, N., Madritsch, H., Guillong, M., Laurent, O., Wohlwend, S., & Bernasconi, S. M. (2021).

402   Absolute age and temperature constraints on deformation along the basal décollement of the

403   Jura fold-and- thrust belt from carbonate U-Pb dating and clumped isotopes. Tectonics, 40,

404   e2020TC006439. https://doi. org/10.1029/2020TC006439

405   Madritsch, H., Schmid, S. M., and Fabbri, O.: Interactions between thin- and thick-skinned tectonics

406   at the northwestern front of the Jura fold-and-thrust belt (eastern France). Tectonics, 27, 1-31,

407   2008.

408   Mazurek, M., Davis, D. W., Madritsch, H., Rufer, D., Villa, I. et al. (2018). Veins in clay-rich

409   aquitards as records of deformation and fluid-flow events in northern Switzerland. Applied

410   Geochemistry, 95, 57-70, 2008.

411   Mazurek, M., Hurford, A. J., and Leu, W.: Unravelling the multi-stage burial history of the Swiss

412   Molasse Basin: integration of apatite fission track, vitrinite reflectance and biomarker

413   isomerisation analysis. Basin Research, 18, 27–50, 2006.

414   Mosar, J.: Present-day and future tectonic underplating in the western Swiss Alps: reconciliation of

415   basement/wrench-faulting and décollement folding of the Jura and Molasse basin in the Alpine

416   foreland. Earth and Planetary Science Letters, 173, 143-155, 1999.

417   Nuriel, P., Weinberger, R., Kylander-Clark, A. R. C., Hacker, B. R., and Craddock, J. P.: The onset

418   of the Dead Sea transform based on calcite age-strain analyses. Geology, 45(7), 587-590, 2017.

419   Parrish, R. R., Parrish, C. M., and Lasalle, S.: Vein calcite dating reveals Pyrenean orogen as cause

420   of Paleogene deformation in southern England. Journal of the Geological Society, 175(3), 425-

421   442, 2018.

422   Philippe, Y., Colletta, B., Deville, E., and Mascle, A.: The Jura fold-and-thrust belt: a kinematic

423   model based on map-balancing. Mémoires du Muséum national d'histoire naturelle, 170, 235-

424   261, 1996.

425   Pfiffner, O. A.: Geology of the Alps. Chichester: John Wiley & Son, 2014.

426   Rime, V., Sommaruga, A., Schori, M., and Mosar, J. : Tectonics of the Neuchâtel Jura Mountains:

427   insights from mapping and forward modelling. Swiss Journal of Geosciences, 112, 563-578,

428   2019.

429   Roberts, N. M., Drost, K., Horstwood, M. S., Condon, D. J., Chew, D., Drake, H., and Haslam, R.:

430   Laser ablation inductively coupled plasma mass spectrometry (LA-ICP-MS) U-Pb carbonate

431   geochronology: strategies, progress, and limitations. Geochronology, 2(1), 33-61, 2020.

432   Roberts, N. M., Žák, J., Vacek, F., and Sláma, J.: No more blind dates with calcite: Fluid-flow vs.

433   fault-slip along the Očkov thrust, Prague Basin. Geoscience Frontiers, 12(4), 101143, 2021.

434   Sissingh, W.: Comparative Tertiary stratigraphy of the Rhine Graben, Bresse Graben and Molasse

435   Basin: correlation of Alpine foreland events. Tectonophysics, 300, 249–28, 1998.

436   Smeraglia, L., Aldega, L., Billi, A., Carminati, E., Di Fiore, F., Gerdes, A., and Vignaroli, G.:

437   Development of an Intrawedge Tectonic Mélange by Out-of-Sequence Thrusting, Buttressing,

438   and Intraformational Rheological Contrast, Mt. Massico Ridge, Apennines, Italy. Tectonics,

439   38(4), 1223-1249, 2019.

440   Smeraglia, L., Fabbri, O., Choulet, F., Buatier, M., Boulvais, P., Bernasconi, S.M., and Castorina, F.:

441   Syntectonic fluid flow and deformation mechanisms within the frontal thrust of foreland fold-

442   and-thrust belt: Example from the Internal Jura, Eastern France. Tectonophysics, 778,

443   https://doi.org/10.1016/j.tecto.2019.228178, 2020.

444   Sommaruga, A.: Geology of the Central Jura and the Molasse basin: New insight into an evaporite-

445   based foreland fold and thrust belt. Mémoires de la Société Neuchâteloise de Sciences

446   Naturelles, 12, pp. 176, 1997.

447   Sommaruga, A., Mosar, J., Schori, M., and Gruber, M.: The role of the Triassic evaporites underneath

448   the North Alpine foreland. In Soto, J., Flinch, J., and Tari, G., (Ed.), Permo- Triassic salt

449   provinces of Europe, North Africa and the Atlantic Margins: tectonics and hydrocarbon

450   potential, chapter 22 (IV). Elsevier, 2017.

451   Thouvenot, F., Fréchet, J., Tapponnier, P., Thomas, J. C., Le Brun, B., Ménard, G., and Paul, A.: The

452   ML 5.3 Epagny (French Alps) earthquake of 1996 July 15: a long-awaited event on the Vuache

453   Fault. Geophysical Journal International, 135(3), 876-892, 1998.

454   Timar-Geng, Z., Fügenschuh, B., Wetzel, A., and Dresmann, H.: The low termperature thermal

455   history of northern Switzerland as revealed by fission track analysis and inverse thermal

456   modelling. Eclogae Geologicae Helvetiae, 99, 255–270, 2006.

457   Twiss, R. J., and Moores, E. M.: Structural geology. Macmillan, 1992.

458   Urai, J. L., Williams, P. F., and Van Roermund, H. L. M.: Kinematics of crystal growth in syntectonic

459   fibrous veins. Journal of Structural Geology, 13(7), 823-836, 1991.

460   Ustaszewski, K., and Schmid, S. M.: Control of preexisting faults on geometry and kinematics in the

461   northernmost part of the Jura fold-and-thrust belt. Tectonics, 25, 1-26, 2006.

462   Van der Pluijm, B. A., Hall, C. M., Vrolijk, P. J., Pevear, D. R., and Covey, M. C.: The dating of

463   shallow faults in the Earth's crust. Nature, 412(6843), 172-175, 2001.

464   Vergés, J., Muñoz, J. A., and Martínez, A.: South Pyrenean fold and thrust belt: The role of foreland

465   evaporitic levels in thrust geometry. In Thrust tectonics, 255-264. Springer, Dordrecht, 1992.

466   Von Hagke, C., Cederbom, C. E., Oncken, O., Stöckli, D. F., Rahn, M. K., and Schlunegger, F.:

467   Linking the northern Alps with their foreland: The latest exhumation history resolved by low-

468   temperature thermochronology. Tectonics, 31(5), 2012.

469   Von Hagke, C., Oncken, O., Ortner, H., Cederbom, C. E., and Aichholzer, S.: Late Miocene to present

470   deformation and erosion of the Central Alps—Evidence for steady state mountain building from

471   thermokinematic data. Tectonophysics, 632, 250-260, 2014.

472   Vrolijk, P., Pevear, D., Covey, M., and LaRiviere, A.: Fault gouge dating: history and evolution. Clay

473   Minerals, 53(3), 305-324, 2018.

474   Woodcock, N. H., Miller, A. V. M., & Woodhouse, C. D.: Chaotic breccia zones on the Pembroke

475   Peninsula, south Wales: Evidence for collapse into voids along dilational faults. Journal of

476   Structural Geology, 69, 91-107, 2014.

477